Exceptionally tight membrane-binding may explain the key role of the synaptotagmin-7 C_2A domain in asynchronous neurotransmitter release

Rashmi Voleti[a,b,c], Diana R. Tomchick[a,b], Thomas C. Südhof[d,e,1], and Josep Rizo[a,b,c,1]

[a]Department of Biophysics, University of Texas Southwestern Medical Center, Dallas, TX 75390; [b]Department of Biochemistry, University of Texas Southwestern Medical Center, Dallas, TX 75390; [c]Department of Pharmacology, University of Texas Southwestern Medical Center, Dallas, TX 75390; [d]Department of Molecular and Cellular Physiology, Stanford University Medical School, Stanford, CA 94305; and [e]Howard Hughes Medical Institute, Stanford University Medical School, Stanford, CA 94305

Contributed by Thomas C. Südhof, August 20, 2017 (sent for review June 16, 2017; reviewed by Rafael Fernandez-Chacon and Mingjie Zhang)

Synaptotagmins (Syts) act as Ca^{2+} sensors in neurotransmitter release by virtue of Ca^{2+}-binding to their two C_2 domains, but their mechanisms of action remain unclear. Puzzlingly, Ca^{2+}-binding to the C_2B domain appears to dominate Syt1 function in synchronous release, whereas Ca^{2+}-binding to the C_2A domain mediates Syt7 function in asynchronous release. Here we show that crystal structures of the Syt7 C_2A domain and C_2AB region, and analyses of intrinsic Ca^{2+}-binding to the Syt7 C2 domains using isothermal titration calorimetry, did not reveal major differences that could explain functional differentiation between Syt7 and Syt1. However, using liposome titrations under Ca^{2+} saturating conditions, we show that the Syt7 C_2A domain has a very high membrane affinity and dominates phospholipid binding to Syt7 in the presence or absence of L-α-phosphatidylinositol 4,5-diphosphate (PIP_2). For Syt1, the two Ca^{2+}-saturated C_2 domains have similar affinities for membranes lacking PIP_2, but the C_2B domain dominates binding to PIP_2-containing membranes. Mutagenesis revealed that the dramatic differences in membrane affinity between the Syt1 and Syt7 C_2A domains arise in part from apparently conservative residue substitutions, showing how striking biochemical and functional differences can result from the cumulative effects of subtle residue substitutions. Viewed together, our results suggest that membrane affinity may be a key determinant of the functions of Syt C_2 domains in neurotransmitter release.

synaptotagmin-7 | synaptotagmin-1 | membrane binding | X-ray crystallography | neurotransmitter release

Neurons communicate with each other via the release of neurotransmitters by synaptic vesicle exocytosis. Neurotransmitter release is triggered by entry of Ca^{2+} into a presynaptic terminal, exhibiting a fast synchronous component that occurs within less than 1 ms after Ca^{2+} influx and a slower, asynchronous component (1). The sophisticated machinery that controls release includes core proteins, such as Munc18-1, Munc13s, and the SNAP receptors (SNAREs) syntaxin-1, SNAP-25, and synaptobrevin, which form a tight SNARE complex that brings the vesicle and plasma membranes together and is key for membrane fusion (2–4). In addition, the exquisite regulation of synaptic exocytosis depends on specialized factors, including the Ca^{2+} sensors from the synaptotagmin (Syt) family (5). Syt1 and the closely related Syt2 and Syt9 act as the Ca^{2+} sensors for the major, synchronous components of neurotransmitter release (6–8), whereas Syt7 mediates at least in part the asynchronous component (9). While major advances have been made in characterizing how all these proteins function, and reconstitution experiments have suggested that basic steps of synaptic vesicle fusion can be recapitulated with eight central proteins (10), fundamental questions remain about the overall mechanism of Ca^{2+}-dependent membrane fusion and in particular about the specific actions of Syts.

Syts contain tandem C_2 domains (referred to as C_2A and C_2B domains) that span most of their cytoplasmic region and adopt characteristic β-sandwich structures (11–13). The Syt1 C_2A and C_2B domains bind three and two Ca^{2+} ions, respectively, through loops at the top of the these β-sandwiches (13–15), which does not cause substantial conformational changes (12) but drastically changes the electrostatic potential of the Ca^{2+}-binding region (13, 15, 16). These top loops also mediate Ca^{2+}-dependent binding to negatively charged phospholipid membranes (17, 18). The key functional importance of this activity was demonstrated by the finding that mutations that increase or decrease the apparent Ca^{2+} affinity of Syt1 in phospholipid binding lead to parallel changes in the Ca^{2+} sensitivity of release (6, 19). The Syt1 C_2B domain can bind simultaneously to two membranes in a Ca^{2+}-dependent manner via the Ca^{2+}-binding loops at the top and two arginines (R398 and R399) at the bottom of the β-sandwich, which may cooperate with SNARE complex formation in bringing the membranes together and inducing membrane fusion upon Ca^{2+} influx (20–22). In support of this model, NMR studies of Syt1–SNARE complex interactions in solution revealed a dynamic binding mode that allows simultaneous interactions with the SNAREs and two closely apposed membranes (23). However, SNARE binding in this structure is mediated by a polybasic region of the C_2B domain that also binds to L-α-phosphatidylinositol 4,5-diphosphate (PIP_2) (24, 25), and

Significance

Synaptotagmins-1 and -7, act as Ca^{2+} sensors for the fast and slow components of neurotransmitter release, respectively, through the two C_2 domains that form their cytoplasmic region. Surprisingly, Ca^{2+}-binding to the synaptotagmin-7 C_2A domain is more critical for slow release than Ca^{2+}-binding to the C_2B domain, whereas the opposite was found for the synaptotagmin-1 C_2 domains and fast release. This paper suggests an explanation for this apparent contradiction, showing that the C_2A domain dominates binding of synaptotagmin-7 to membranes, whereas such binding is dominated by the C_2B domain in the case of synaptotagmin-1. Thus, membrane affinity may be a key determinant of the relative functional importance of synaptotagmin C_2 domains.

Author contributions: R.V., D.R.T., T.C.S., and J.R. designed research; R.V. and D.R.T. performed research; R.V., D.R.T., T.C.S., and J.R. analyzed data; and R.V., D.R.T., T.C.S., and J.R. wrote the paper.

Reviewers: R.F.-C., University of Seville; and M.Z., Hong Kong University of Science and Technology.

The authors declare no conflict of interest.

Data deposition: The atomic coordinates and structure factors have been deposited in the Protein Data Bank, www.wwpdb.org [PDB ID codes 6ANJ (Syt7 C2A domain) and 6ANK (Syt7 C2AB fragment)].

[1]To whom correspondence may be addressed. Email: tcs1@stanford.edu or jose.rizo-rey@UTSouthwestern.edu.

This article contains supporting information online at www.pnas.org/lookup/suppl/doi:10.1073/pnas.1710708114/-/DCSupplemental.

multiple Syt1–SNARE complex binding modes likely exist (23). Indeed, a crystal structure revealed three different Syt1–SNARE complex binding modes, all distinct from that observed in solution (26). Hence, it is still unclear how the functions of Syt1 and the SNARE complex are coupled.

The structural and biochemical properties uncovered by the extensive studies of the Syt1 C_2 domains are paradigmatic in general terms for C_2 domains of other Ca^{2+}-dependent Syts, but differences in these properties can range from subtle to dramatic (5). Such differences can be difficult to predict from sequence alignments alone (e.g., ref. 27) and can result in fine or drastic functional differences that may also be difficult to rationalize from sequence analyses. Particularly intriguing in this respect are the differences between Syt1 and Syt7, as both isoforms function as Ca^{2+} sensors for exocytosis in chromaffin cells (28) and presynaptic terminals (6, 9), but Syt7 cannot functionally replace Syt1 to trigger fast synchronous neurotransmitter release (8). In fact, replacing the C_2B domain in Syt1 with the Syt7 C_2B domain prevents rescue of synchronous release in Syt1 KO neurons even after extensive mutagenesis to replace residues of the Syt7 C_2B domain back with those present in Syt1 (29). The crystal structure of the Syt7 C_2B domain did not reveal substantial differences from that of the Syt1 C_2B domain that could clarify the basis for these results (29). Moreover, mutating the Ca^{2+}-binding sites of the Syt1 C_2B domain impairs synchronous release much more drastically than analogous mutations in the Ca^{2+}-binding sites of the Syt1 C_2A domain (30–33), whereas asynchronous release is more strongly impaired by mutations in the Ca^{2+}-binding sites of the Syt7 C_2A domain than mutations in the Syt7 C_2B domain Ca^{2+}-binding sites (9). In principle, these results suggest that the relative functional importance of the two C_2 domains is switched in Syt1 and Syt7, but this conclusion represents a simplification because substitutions in the C_2B domain Ca^{2+}-binding sites render Syt1 dominant-negative (30, 34). Strikingly, expressing such mutant Syt1 in WT cells blocks both synchronous and asynchronous Ca^{2+}-triggered release, suggesting that C2B-domain mutant Syt1 locks synaptic vesicles into a Ca^{2+}-unresponsive state. Overall, these findings show that understanding the key determinants for functional differentiation between Syt1 and Syt7 remains as a major challenge in this field.

In the study presented herein, we have investigated the structural and biochemical basis for the differences in the relative functional importance of Ca^{2+}-binding to the Syt7 C_2 domains. We have determined crystal structures of the Syt7 C_2A domain and of a fragment spanning the two Syt7 C_2 domains (C_2AB), and found no structural features that could readily explain their distinct functional properties. Isothermal titration calorimetry (ITC) data reveal that the intrinsic Ca^{2+} affinities of the Syt7 C_2 domains are similar to those of the Syt1 C_2 domains. However, in contrast to Syt1, we find that under Ca^{2+} saturating conditions the Syt7 C_2A domain binds to phospholipids with much higher affinity than the Syt7 C_2B domain, and that disruption of the C_2A domain Ca^{2+}-binding sites impairs binding of the Syt7 C_2AB fragment to phospholipids more strongly than disruption of the C_2B domain Ca^{2+}-binding sites. Moreover, the Ca^{2+}-saturated Syt7 C_2A domain clusters liposomes and hence has the ability to bring two membranes together, whereas the Syt7 C_2B domain does not, again in contrast to results obtained with Syt1. These results suggest that the dominant function of Ca^{2+} binding to the Syt7 C_2A domain versus the C_2B domain in asynchronous release arises because of its preponderant role in membrane binding and perhaps in bringing the vesicle and plasma membranes together. Furthermore, mutagenesis shows that cooperative effects of apparently conservative amino acid substitutions underlie at least in part the much higher phospholipid binding affinity of the Syt7 C_2A domain compared with the Syt1 C_2A domain, illustrating how the cumulative effects of subtle mutations can have profound effects in protein biochemistry and function.

Results

Crystal Structure of the Ca^{2+}-Bound Syt7 C2A Domain. The crystal structure of the Ca^{2+}-bound Syt7 C_2B domain has been determined and found to be very similar to that of the Syt1 C_2B domain, although three Ca^{2+}-binding sites were observed in the Syt7 C_2B domain instead of two (29). A solution structure of the Ca^{2+}-free Syt7 C_2A domain determined by NMR spectroscopy was deposited in the Protein Data Bank as part of a structural genomics initiative (PDB ID code 2D8K). To investigate whether Ca^{2+} induces conformational changes in the Syt7 C_2A domain, we performed crystallization screens in the presence of Ca^{2+} and were able to obtain crystals that diffracted to 1.7 Å. The structure of the Ca^{2+}-bound Syt7 C_2A domain was determined by molecular replacement using the Ca^{2+}-free solution structure as the search model. Data collection and refinement statistics are described in Table S1.

Fig. 1*A* shows the ribbon diagram of the Ca^{2+}-bound Syt7 C2A domain, which has a typical β-sandwich architecture composed of two four-stranded β-sheets characteristic of C_2 domains (35). The structure is very similar to the Ca^{2+}-free solution structure (Fig. 1*B*), with a 1.13 Å rmsd for 127 equivalent Cα carbons. Differences observed in some of the loops can readily arise from the known flexibility of these loops in C_2 domains (12, 35) and potential adaptations induced by crystal contacts. Hence, Ca^{2+} binding does not appear to induce substantial structural changes in the Syt7 C_2A domain, as observed for the Syt1 C_2A domain (12). Indeed, the structures of the Ca^{2+}-bound C_2A domains of Syt1 and Syt7 are also very similar (Fig. 1*C*), with a 0.92 Å rmsd for 113 equivalent Cα carbons. Note that the perturbations induced by Ca^{2+} in the ^1H-^{15}N heteronuclear single quantum coherence (HSQC) spectra of the Syt7 C_2A domain (36) are also

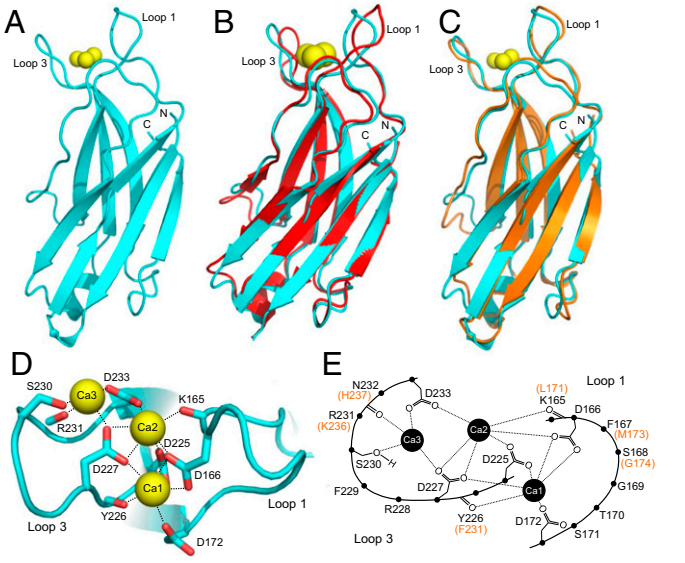

Fig. 1. Crystal structure of the Ca^{2+}-bound Syt7 C_2A domain. (*A*) Ribbon diagram of the crystal structure of the Ca^{2+}-bound Syt7 C_2A domain. The three bound Ca^{2+} ions are shown as yellow spheres. The two loops involved in Ca^{2+} binding are indicated (loop 1 and loop 3), and the N and C termini are labeled N and C, respectively. (*B*) Superposition of the crystal structure of the Ca^{2+}-bound Syt7 C_2A domain (cyan) with the solution structure of Ca^{2+}-free Syt7 C_2A domain (red) (PDB ID code 2D8K). (*C*) Superposition of the crystal structure of the Ca^{2+}-bound Syt7 C_2A domain (cyan) with the solution structure of Ca^{2+}-bound Syt1 C_2A domain (orange) (PDB ID code 1BYN). (*D*) Diagram illustrating the Ca^{2+}-binding sites of the Syt7 C_2A domain. The three bound Ca^{2+} ions are labeled Ca1, Ca2, and Ca3. The Ca^{2+} ligands are shown as stick models and labeled. (*E*) Diagram of the Ca^{2+}-binding sites of Syt7 C_2A domain summarizing all of the residues in loops 1 and 3 (black letters). The residues that are different in the Syt1 C_2A domain are indicated in parenthesis in red letters.

comparable to those observed for the Syt1 C_2A domain (15). Correspondingly, the Syt7 C_2A domain binds three Ca^{2+} ions via the same ligands (Fig. 1 *D* and *E*) observed in the three Ca^{2+}-binding sites of the Syt1 C_2A domain (12, 15). Overall, these results show that there are no overt differences in the structure and Ca^{2+}-binding mode of the C_2A domains from Syt1 and Syt7 that might explain the predominant role of Ca^{2+} binding to the Syt7 C_2A domain in asynchronous neurotransmitter release.

Crystal Structure of the Syt7 C2AB Fragment. A crystal structure of a Syt1 C_2AB fragment in the absence of Ca^{2+} revealed extensive contacts between the two C_2 domains that distort the Ca^{2+}-binding region of the C_2A domain and hence would be expected to be disrupted upon Ca^{2+} binding to this domain, which could provide a mechanism for Ca^{2+}-regulation of neurotransmitter release (37). Although such contacts did not appear to occur in solution (20), we performed extensive crystallization screens with the Syt7 C_2AB fragment to examine the possibility of intramolecular interactions between the two Syt7 C_2 domains. Unfortunately, we were not able to obtain crystals for Ca^{2+}-free Syt7 C_2AB, but we did obtain crystals in the presence of Ca^{2+} and we determined its structure by molecular replacement using the crystal structures of the Syt7 C_2A and C_2B domains (Fig. 1*A* and ref. 29) as search models (Fig. 2*A*). Data collection and refinement statistics are summarized in Table S1.

The structures of the two C_2 domains in the Syt7 C_2AB structure are very similar to those observed in the crystal structures of the isolated C_2A (described above) and C_2B (29) domains. Comparison of the isolated C_2A domain with this domain in the two structures of C_2AB in the asymmetric unit of its crystals revealed rmsds of 0.49 and 0.58 Å for 125 equivalent Cα carbons, whereas for the C_2B domain the rmsds were 0.45 and 0.41 Å for 138 and 137 equivalent Cα carbons, respectively. No density could be modeled for the linker sequence between the two C_2 domains in the structure of the Syt7 C_2AB fragment, and the observed contacts between the domains were typical of crystal packing interfaces, suggesting that the relative orientation between the two C_2 domains is a result of crystal packing. Comparison of the crystal structure of Syt7 C_2AB with those of isolated Syt1 C_2AB (37), one of the C_2AB molecules in the crystal structure of Syt1 C_2AB bound to the SNARE complex (26) and the crystal structure of Syt3 C_2AB (38), shows that the relative orientation of the two C_2 domains is very different in each structure (Fig. 2*B*), supporting the conclusion drawn from NMR studies of Syt1 C_2AB that this relative orientation is flexible, and hence adaptable (20). We also analyzed the Syt7 C_2AB fragment by NMR spectroscopy and found that its ^1H-^{15}N HSQC spectra in the presence and absence of Ca^{2+} are very similar to the superposition of ^1H-^{15}N HSQC acquired separately for the isolated C_2A and C_2B domains (Fig. S1). There are a few cross-peaks that do not overlap, but they can be attributed to residues from the linker or adjacent sequences, and the overall coincidence of cross-peaks is inconsistent with extensive contacts between the two C_2 domains, thus supporting the conclusion that their relative orientation is flexible.

Intrinsic Calcium Binding to the Syt7 C_2A and C_2B Domains. In the crystal structure of the Syt7 C_2AB fragment we observed only two Ca^{2+} ions bound to the C_2A domain and two Ca^{2+} ions bound to the C_2B domain (Fig. 2*A*), corresponding in both cases to sites Ca1 and Ca2 as defined for the C_2A domain in Fig. 1*E*. These findings contrast with the observation of three bound Ca^{2+} ions in the structure of the isolated Syt7 C_2A domain (Fig. 1*D*) and four bound Ca^{2+} ions in the crystal structure of the isolated C_2B domain (29). These differences are not surprising, as the third Ca^{2+}-binding site observed in the isolated Syt7 C_2A domain (Ca3) is likely of lower affinity because it is formed by only four protein ligands (Fig. 1*D*) and, in the final refined structure, Ca3 displayed a higher *B*-factor (11.8 $Å^2$) than Ca1 (7.8 $Å^2$) or Ca2 (7.2 $Å^2$). The Ca3 site may not be occupied in the crystals of the Syt7 C_2AB fragment because of the high sulfate concentration present in the crystallization conditions. For the isolated Syt7 C_2B domain, one of the two additional Ca^{2+} ions was bound to site Ca3, which is also formed by four protein ligands, and the other was bound to an additional site formed by only three protein ligands on the outside of the cup shape formed by the Ca^{2+}-binding loops, near a lattice contact (29). In the final refined Syt7 C_2B structure, Ca3 also displayed a higher *B*-factor (16.2 $Å^2$) than Ca1 (8.8 $Å^2$) or Ca2 (10.1 $Å^2$). Although the crystals of the isolated Syt7 C_2B domain also contained high sulfate concentration, the lower pH used to crystalize the Syt7 C_2AB fragment (6.0 instead of 6.5) may have decreased the already weak Ca^{2+} affinity of these two sites and, hence, no binding is observed.

To analyze the intrinsic affinities of the Ca^{2+}-binding sites of the Syt7 C_2 domains in solution, we used ITC (Fig. 3). For this purpose, we used the isolated Syt7 C_2A and C_2B domains because the expected existence of multiple Ca^{2+} binding sites would hinder fitting the data obtained with the C_2AB fragment, and because the

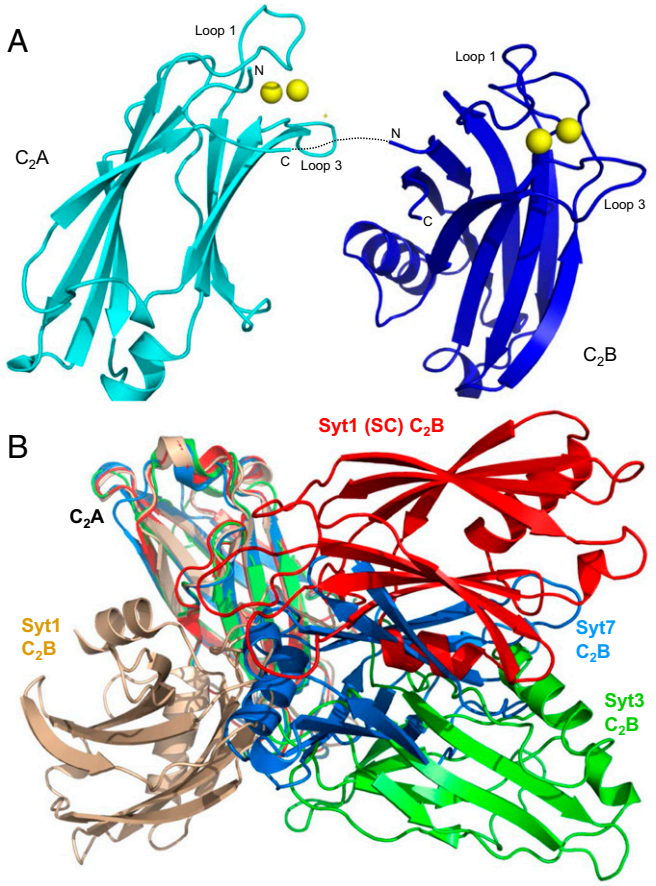

Fig. 2. Crystal structure of the Ca^{2+}-bound Syt7 C_2AB fragment. (*A*) Ribbon diagram of the crystal structure of the Ca^{2+}-bound Syt7 C_2AB fragment, with the C_2A domain in cyan and the C_2B domain in blue. The bound Ca^{2+} ions are shown as yellow spheres. The loops involved in Ca^{2+} binding are indicated (loop 1 and loop 3), and the N and C termini of both domains are labeled N and C, respectively. The sequence linking the two C_2 domains, for which there is insufficient electronic density to build the structure, is illustrated by a dotted line. (*B*) Superposition of the crystal structure of the Ca^{2+}-bound Syt7 C_2AB (cyan and blue) with the crystal structures of Ca^{2+}-free Syt1 C_2AB (wheat; PDB ID code 2R83), Syt1 C_2AB bound to the SNARE complex (red; PDB ID code 5CCG) and Ca^{2+}-free Syt3 C_2AB (green; PDB ID code 1DQV). Only the C_2A domain of each structure was used for the superposition to illustrate the diversity of relative orientations between the two C_2 domains in these structures. The position of all of the C_2A domains is indicated by C_2A and those of the different C_2B domains are also labeled; Syt1 (SC) C_2B domain refers to Syt1 C_2AB bound to the SNARE complex.

two C_2 domains are not expected to influence each other in Ca^{2+} binding given their flexible relative orientation. We found that fitting the ITC data obtained for the Syt7 C_2A domain (Fig. 3*A*) required a three-sequential-binding-site model, consistent with the crystal structure of the isolated domain (Fig. 1*A*). The K_Ds measured for the three Ca^{2+} binding sites were 90 ± 15 μM, 180 ± 42 μM, and 11 ± 5 mM. These K_Ds should be examined with caution due to the natural difficulty in obtaining accurate K_Ds from such multiple binding-site data, but it is reassuring that the values are comparable to those measured previously by NMR spectroscopy for the Syt7 C_2A domain (~150 μM, 200–300 μM and >2 mM) (36). They are also similar to K_Ds obtained for the Syt1 C_2A domain by NMR spectroscopy (54 μM, 530 μM and >2 mM) (6) and ITC (119 μM, 465 μM and 1.7 mM) (39).

Fitting the ITC data obtained for the Syt7 C_2B domain required a four-sequential-binding-site model, as attempts to fit the data assuming only three binding sites yielded a systematic error at the end of the titration, which reflects binding to a very low-affinity Ca^{2+}-binding site. Hence, these data are consistent with the crystal structure of the isolated Syt7 C_2B domain (29). Unfortunately, it was difficult to obtain reliable K_Ds from these data because of the multiplicity of binding sites and because the values obtained depended strongly on the position chosen for the zero baseline (note the drift observed even at molar ratio = 40) (Fig. 3*B*). Nevertheless, the ranges of K_D values for the four sites (75–900 μM, 0.5–1.2 mM, 3–5 mM, and 5–27 mM) obtained in different fits give an idea of the intrinsic affinities of the four sites. The K_Ds of the two higher affinity sites are comparable to those of the two Ca^{2+}-binding sites of the Syt1 C_2B domain, for which NMR data yielded estimated K_Ds of 300–400 and 500–600 μM (13) and ITC experiments yielded an estimated overall K_D of 200 μM for the two sites (39). It is currently unclear whether all four Ca^{2+}-binding sites of the Syt7 C_2B domain, or perhaps only three or two, are physiologically relevant but, regardless of these possibilities, these results indicate that the intrinsic Ca^{2+}-binding properties of the C_2 domains from Syt7 are similar to those of the Syt1 C_2 domains and do not provide an explanation for the differences in the relative functional importance of the Syt7 C_2 domains.

The Ca^{2+}-Bound Syt7 C_2A Domain Binds to Membranes with Higher Affinity than the Ca^{2+}-Bound C_2B Domain. The apparent Ca^{2+} affinities of Syt C_2 domains in Ca^{2+}-dependent phospholipid binding assays are much stronger (apparent K_Ds < 10 μM) than their intrinsic Ca^{2+} affinities because the phospholipids contribute to coordinate the bound Ca^{2+} ions (6, 17, 40). Notably, the apparent Ca^{2+}-affinity of the Syt7 C_2A domain in Ca^{2+}-dependent phospholipid binding is considerably higher than that of the Syt1 C_2A domain (40). This higher apparent Ca^{2+} affinity can be associated to slower dissociation rates from the membranes (41), which has been also observed in experiments performed with Syt1 and Syt7 C_2AB fragments (42). Since the intrinsic Ca^{2+} affinities of the Syt1 and Syt7 C_2 domains are similar, their differences in Ca^{2+}-dependent phospholipid binding can be ascribed to stronger interactions with the membranes in the Ca^{2+}-bound state. Thus, we decided to investigate whether differences in membrane affinity might underlie the relative contributions of the C_2A and C_2B domains to Syt7 function. For this purpose, we used a similar approach to that described previously for the Syt1 C_2 domains, which used FRET to detect phospholipid binding and titrations with liposomes under Ca^{2+} saturating conditions to compare relative membrane affinities (39).

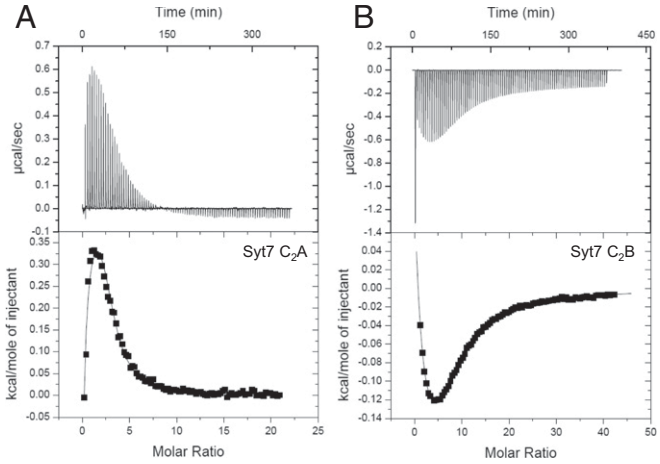

Fig. 3. ITC analysis of intrinsic Ca^{2+} binding to the Syt7 C_2 domains. Illustrative ITC data obtained by titration of Ca^{2+} versus the isolated Syt7 C_2A (*A*) or C_2B (*B*) domain. The curves represent the fits of the data to a three- (*A*) or four- (*B*) sequential-binding-site model.

In our FRET assays, we used liposomes containing Rhodamine-PE as a FRET acceptor and a BODIPY-FL donor probe was attached to the native cysteines of the Syt7 C_2A and C_2B domain (C260 and C275, respectively), which are located in regions that are not expected to participate in phospholipid binding based on extensive analyses of Syt1 (e.g., refs. 17, 18, 43, and 44) (Fig. S2*A*). For experiments with the Syt7 C_2AB fragment, the BODIPY-FL probe was attached to either C260 or C275 (indicated by an asterisk; i.e., C_2A*B or C_2AB*) and the other cysteine was mutated to alanine. The position of the probe did not substantially alter the phospholipid binding curves (Fig. S2*B*). Most of the data shown were obtained with the probe on C260 of the C_2A domain, except for experiments where the Ca^{2+}-binding sites of the C_2A domain were mutated, in which case the probe was attached to C275 of the C_2B domain. In initial experiments and those described below for Syt1 fragments, we performed titrations with increasing amounts of liposomes onto 100 nM protein under Ca^{2+} saturating conditions. However, because of the very high liposome affinities observed for fragments including the Syt7 C_2A domain, we lowered the protein concentration to 20 nM to allow better discrimination of relative liposome affinities. Even at these low protein concentrations, excellent consistency was observed in separate experiments performed under the same conditions with different liposome preparations (e.g., Fig. S2 *D* and *E*). All of the data could be fit well to a Hill function (Figs. 4–7), with Hill coefficients ranging from 1 to 3 (Table 1) that in principle could indicate some cooperativity. However, it is important to note that it is difficult to interpret Hill coefficients in these experiments because at low concentrations of liposomes (high protein-to-lipid ratios) their surface may be covered by bound proteins, which is expected to occlude some of the available binding sites because of molecular crowding and at the same time can favor liposome clustering. On the opposite end, at high liposome concentrations (low protein-to-lipid ratios) molecular crowding effects are not expected and liposome clustering is less favorable (20). Hence, we did not attempt to rationalize the Hill coefficients and only used the K_Ds derived from fitting the data (Table 1) as apparent values that report on the relative affinities of the Ca^{2+}-saturated proteins for the liposomes.

We first used liposomes containing a lipid composition that resembles that of physiological membranes (33) but did not include PIP_2 (Fig. 4). Importantly, liposome titrations revealed that the Syt7 C_2A domain binds with much higher affinity than the Syt7 C_2B domain and a similar affinity to that observed for Syt7 C_2AB (Fig. 4 *A* and *B* and Table 1). In fact, the curves observed for Syt7 C_2AB were consistently shifted to the right (i.e., larger K_D) compared with those obtained for the Syt7 C_2A domain (Fig. 4*B*), but this observation does not necessarily imply a higher affinity of the C_2A domain versus C_2AB. Considering that a C_2 domain can bind multiple phospholipids and has a much larger area than that of a phospholipid headgroup, that the liposomes contained 17% of negatively charged phospholipids,

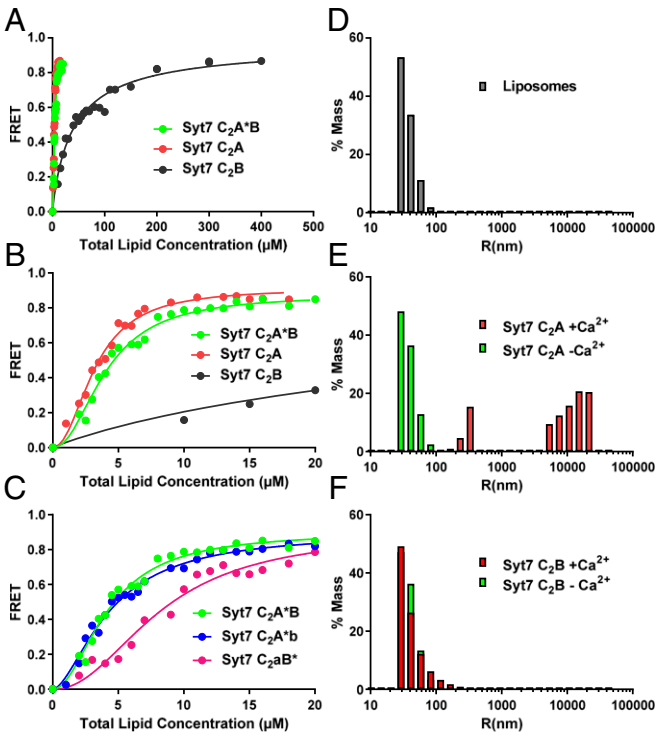

Fig. 4. The Syt7 C_2A domain dominates binding of Syt7 to membranes and clusters liposomes. (*A*) Titrations of 20 nM Syt7 C_2A domain, C_2B domain and C_2A*B fragment (the * in C_2A*B denotes that the fluorescent probe is attached to C260 of the C_2A domain) with liposomes lacking PIP_2 in the presence of 1 mM Ca^{2+}. Binding was monitored from the FRET developed between a donor BODIPY-FL probe attached to the proteins and a rhodamine acceptor present in the liposomes. Each point represents the average of at least three measurements performed with different liposome preparations. (*B*) The same titrations shown in *A* but changing the *x* axis to better show the points of the titrations obtained at low liposome concentrations. (*C*) Liposome titrations of 20 nM WT Syt7 C_2AB fragment and mutant fragments where the Ca^{2+}-binding sites of the C_2A domain (C_2aB*) or C_2B domain (C_2A*b) were disrupted with D225A,D227A,D233A or D357A,D359A mutations. All of the data in *A*–*C* were fit to a Hill function. (*D*–*F*) Distribution of particle size measured by DLS on samples containing liposomes alone (*D*) or liposomes in the presence of the Syt7 C_2A domain (*E*) or Syt7 C_2B domain (*F*). In *E* and *F*, the diagrams show superpositions of data obtained in the absence (green bars) or presence (red bars) of Ca^{2+}.

that only half of the lipids are in the outer leaflets, and that molecular crowding limits the availability of more than 70% of the liposome surface (20), the amounts of phospholipids required to observed maximum FRET for the Syt7 C_2A domain and C_2AB fragment suggest that we are observing saturation binding curves. Hence, the right shift of the curves observed for the Syt7 C_2AB fragment compared with the C_2A domain most likely reflects the fact that C_2AB is larger than C_2A, thus requiring more lipids for quantitative binding. We also performed titrations with Syt7 C_2AB fragments containing mutations that disrupt the Ca^{2+}-binding sites of the C_2A domain (denoted C_2aB* because C_2A cannot bind Ca^{2+} and the fluorescent probe is on C_2B) or the C_2B domain (C_2A*b). Interestingly, impairing Ca^{2+}-binding to the C_2A domain markedly decreased the membrane affinity of Syt7 C_2AB, whereas disrupting Ca^{2+} binding to the C_2B domain had little effect (Fig. 4*C* and Table 1). These results show that the C_2A domain dominates binding of Syt7 to membranes and reveal a clear correlation with the finding that disrupting Ca^{2+} binding to the C_2A domain has a much stronger effect on the function of Syt7 in asynchronous release than abrogating Ca^{2+} binding to the C_2B domain (9).

The Ca^{2+}-Bound Syt7 C_2A Domain Has Higher Membrane-Bridging Activity than the Ca^{2+}-Bound C_2B Domain. The finding that the Syt1 C_2B domain can bridge two membranes, bringing them into close proximity, suggested that this property could be crucial for Syt1 function and could explain the critical functional importance of Ca^{2+}-binding to the Syt1 C_2B domain (20, 22). Thus, we also tested the membrane bridging activity of the Syt7 C_2 domains. For this purpose, we analyzed the formation of liposome clusters due to membrane bridging using dynamic light scattering (DLS). Isolated liposomes had radii below 100 nm (Fig. 4*D*) that did not change substantially upon addition of the Syt7 C_2A domain or C_2B domain in the absence of Ca^{2+} (Fig. 4 *E* and *F*). However, in the presence of Ca^{2+}, the Syt7 C_2A domain caused a dramatic increase in particle size reflecting robust vesicle clustering, whereas the C_2B domain had practically no activity (Fig. 4 *E* and *F*). These results again correlate with the electrophysiological data and suggest that the preponderant role of Ca^{2+} binding to the Syt7 C_2A domain in triggering asynchronous release may arise not only from its the higher membrane affinity, compared with the C_2B domain, but also from its stronger ability to bridge two membranes.

The Ca^{2+}-Bound Syt1 C_2B Domain Binds to PIP_2-Containing Membranes with Higher Affinity than the Ca^{2+}-Bound Syt1 C_2A Domain. Phospholipid binding to the Syt1 C_2 domains has been extensively investigated (1, 45, 46), but most studies analyzed the Ca^{2+} dependence of lipid binding, and analysis of phospholipid binding under Ca^{2+} saturating conditions was mostly focused on Syt1 C_2AB fragments (39). To compare the properties of the Syt1 C_2 domains using the same methodology used for our experiments with the Syt7 C_2 domains and examine whether the asymmetry in the functional importance of Ca^{2+}-binding to the Syt1 C_2 domains may also be reflected in their membrane affinities, we performed liposome titrations of the Ca^{2+}-saturated Syt1 C_2A domain, C_2B domain, and C_2AB fragment. Because the Syt1 C_2 domains only contain one cysteine side chain (C277) and this side chain is buried, we mutated this cysteine to alanine and introduced single cysteine mutations in regions of the C_2A and C_2B domain that have not been implicated in lipid binding (Fig. S2*A*). As in the case of Syt7 C_2AB, placing the fluorescent probe on the C_2A or C_2B domain did not substantially affect the phospholipid curves observed for the Syt1 C_2AB fragment (Fig. S2*C*).

Our data showed that the Ca^{2+}-saturated Syt1 C_2A and C_2B domains bind to the liposomes with similar affinities, which were

Table 1. Apparent liposome affinities of Ca^{2+}-saturated Syt7 and Syt1 C_2 domain fragments

Protein fragment	K_D (μM)	SD	*h*	SD
Syt7 C_2A	2.40	0.54	2.18	0.41
Syt7 C_2B	34.97	2.92	1.02	0.09
Syt7 C_2A*B	4.12	0.80	3.1	0.52
Syt7 C_2A*b	4.29	0.18	1.74	0.26
Syt7 C_2aB*	8.06	0.39	2.03	0.26
Syt7 C_2A F167M,R231K	8.68	0.44	1.61	0.17
Syt1 C_2A	551.1	134.26	1.34	0.159
Syt1 C_2B	637.37	146.89	1.78	0.38
Syt1 C_2A*B	24.05	1.77	2.15	0.46
Syt1 C2A*b	245.5	4.49	1.95	0.24
Syt1 C_2aB*	267.23	38.96	2.09	0.25
Syt1 C_2A M173F,K236R	95.48	25.9	1.51	0.3

The listed apparent K_Ds and Hill coefficients (h), as well as their SDs, were obtained from fitting the FRET data obtained in liposome titrations of the indicated Ca^{2+}-saturated Syt7 and Syt1 C_2 domain fragments. At least three titrations were performed for each fragment. K_Ds and *h* values were derived for each titration, and the averages as well as SDs were calculated. The protein concentrations were 20 nM for all Syt7 fragments and 100 nM for all Syt1 fragments.

much weaker than that observed for the Syt7 C_2A domain and were far from leading to saturation binding curves (Fig. 5*A*). Syt1 C_2AB bound much more avidly than the individual Syt1 C_2 domains (Fig. 5 *A* and *B* and Table 1), showing that they cooperate strongly in membrane binding. Mutation of the Ca^{2+}-binding sites of the C_2A or C_2B domain considerably impaired phospholipid binding to the Syt1 C_2AB fragment, but to similar extents (Fig. 5*C*) that do not correlate with the stronger disruption of Syt1 function caused by mutation of the C_2B domain Ca^{2+}-binding sites.

Because PIP_2 is known to increase the membrane affinity of the C_2B domain but not the C_2A domain (47), we performed additional experiments with liposomes that contained the same lipid composition except for the inclusion of 1% PIP_2. Our data confirmed that, indeed, the presence of PIP_2 in the liposomes did not alter the affinity for the Syt1 C_2A domain but dramatically increased the affinity for the Syt1 C_2B domain (Fig. 6 *A* and *B*). Hence, in the presence of PIP_2, the stronger membrane affinity of the Ca^{2+}-saturated Syt1 C_2B domain compared with the C_2A domain does correlate with the functional effects of disrupting Ca^{2+} binding. These results led us to also test the effects of including PIP_2 on the membrane affinity of the Syt7 C_2 domains. PIP_2 clearly increased the membrane affinity of the Syt7 C_2B domain but did not appear to alter liposome binding to the Syt7 C_2A domain (Fig. 6 *C* and *D*). However, the latter result needs to be interpreted with caution because the titrations with Syt7 C_2A domain most likely reflect saturation binding (see above), which is expected to prevent observation of any increase in membrane affinity due to inclusion of PIP_2. Note also that, even in the presence of PIP_2, the Ca^{2+}-saturated Syt7 C_2A domain still binds membranes with higher affinity than the Syt7 C_2B domain (Fig. S3).

Subtle Residue Substitutions Underlie in Part the Differential Membrane Affinities of the Syt1 and Syt7 C_2A Domains. Overall, the data presented above and other previous results suggest that phospholipid binding affinity is a key factor that determines the functional importance of Syt C_2 domains. When comparing the properties of Syt1 and Syt7, it is particularly striking that the Syt7 C_2A domain has such a higher membrane-binding affinity than the Syt1 C_2A domain (Figs. 4 and 5), with an apparent K_D at least 200 times smaller (Table 1). This finding is not surprising given previous results showing a higher apparent Ca^{2+} affinity (40) and a slower membrane dissociation rate (41) for the Syt7 C_2A domain compared with the Syt1 C_2A domain, but it seems difficult to rationalize considering the similarities of the 3D structures, the intrinsic Ca^{2+} affinities, and the sequences of these domains. Given the key functional importance of membrane binding, elucidating the sequence determinants of membrane affinity is critical to understand the functional differences between Syts, and the C_2A domains of Syt1 and Syt7 provide an ideal benchmark to address this question.

We hypothesized that differences in the membrane affinities of the two domains arise because of cumulative small or moderate effects caused by residues that are distinct in the Ca^{2+}-binding regions of the Syt1 and Syt7 C_2A domains. To test this hypothesis, we prepared six single-site mutants of the Syt7 C_2A domain where single residues were replaced by the (distinct) residue present in the homologous position of the Syt1 C_2A domain (Fig. 7*A*; see also Fig. 1*E*). Titrations with liposomes under Ca^{2+} saturating conditions did not reveal substantial differences between the membrane affinities of any of the single mutants and the WT Syt7 C_2A domain (Fig. 7 *B* and *C*). We reasoned that perhaps some of these single site mutations decreased the membrane affinity of the Syt7 C_2A domain but, since the WT affinity is so high, a modest decrease in affinity may not be observable because the experiments still yield saturation binding curves. To try to cause a stronger decrease in membrane affinity that may be observable, we combined two of the single mutations (F167M and R231K) into a double mutant. Note that these mutations would normally be considered conservative, but they might decrease membrane affinity to some extent because arginines can form hydrogen bonds more efficiently with phosphate groups than lysines, and phenylalanines have a larger hydrophobic surface than methionines. Indeed, the double F167M, R231K mutation markedly impaired liposome binding to the Syt7 C_2A domain (Fig. 7*C* and Table 1).

If the differences in membrane affinities between the Syt1 and Syt7 C_2A domains arise in part because of the nature of these two side chains, rather than differences in 3D structure or intrinsic Ca^{2+}

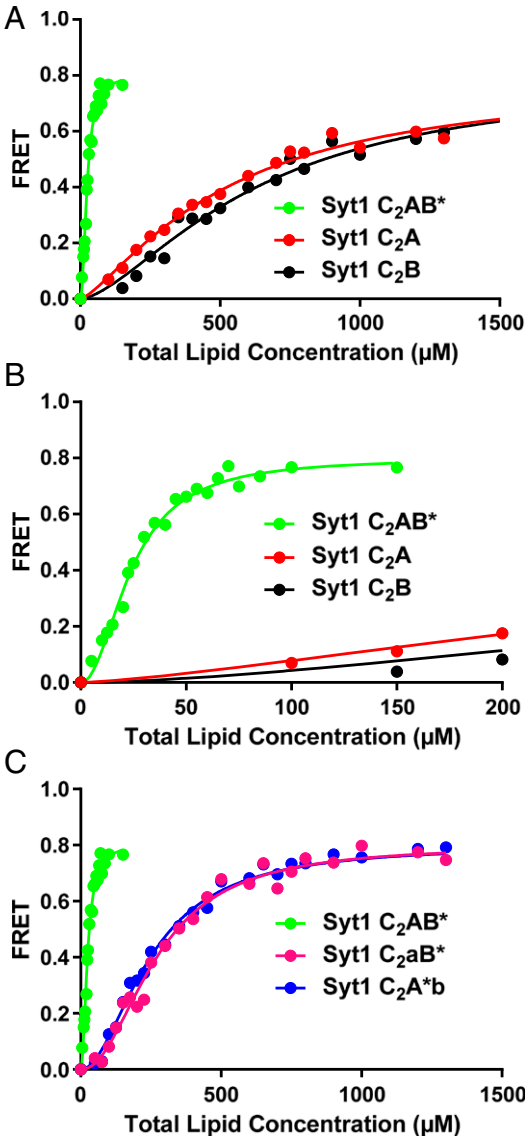

Fig. 5. The Syt1 C_2 domains have similar membrane affinities and cooperate in membrane binding. (*A*) Titrations of 100 nM Syt1 C_2A domain, C_2B domain and C_2AB* fragment (the * in C_2AB* denotes that the fluorescent probe is attached to the C_2B domain) with liposomes lacking PIP_2 in the presence of 1 mM Ca^{2+}. Binding was monitored from the FRET developed between a donor BODIPY-FL probe attached to the proteins and a rhodamine acceptor present in the liposomes. Each point represents the average of at least three measurements performed with different liposome preparations. (*B*) The same titrations shown in *A* but changing the *x* axis to better show the points of the titrations obtained at low liposome concentrations. (*C*) Liposome titrations of 100 nM WT Syt1 C_2AB* fragment and mutant fragments where the Ca^{2+}-binding sites of the C_2A domain (C_2aB*) or C_2B domain (C_2A*b) were disrupted with D178A,D230A,D232A or D309A,D363A,D365A mutations. All of the data were fit to a Hill function.

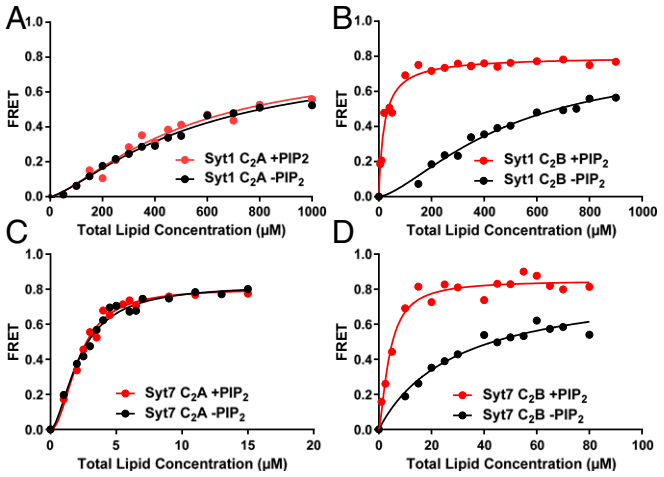

Fig. 6. PIP_2 enhances the membrane affinity of the Syt1 and Syt7 C_2B domains. Titrations of 100 nM Syt1 C_2A domain (*A*) or C_2B domain (*B*), or 20 nM Syt7 C_2A domain (*C*) and C_2B domain (*D*) with liposomes lacking (black circles) or containing (red circles) PIP_2 in the presence of 1 mM Ca^{2+}. Binding was monitored from the FRET developed between a donor BODIPY-FL probe attached to the proteins and a rhodamine acceptor present in the liposomes. Each point represents the average of at least three measurements performed with different liposome preparations. All of the data were fit to a Hill function.

affinities, we could expect that making the reverse mutations in the Syt1 C_2A domain would increase its membrane affinity. Indeed, single M173F and K236R mutations both increased the membrane affinity of the Syt1 C_2A domain, and a double M173F,K236R mutation revealed an additional increase in membrane affinity that reflects the cumulative effects of the two mutations (Fig. 7*D*). Titrations of Syt1 and Syt7 fragments were generally performed at 100 nM and 20 nM protein concentrations, respectively, to better dissect the differences in membrane affinities between the fragments of each isoform. To be able to directly compare the membrane affinities of the Syt1 and Syt7 C_2A domains in this set of experiments, we repeated the titrations of the WT and F167M, R231K mutant Syt7 C_2A domain at 100 nM protein concentration. Comparison of the results with those obtained for the WT and M173F,K236R Syt1 C_2A domains (Fig. 7*E*) showed that the Syt7 double mutant still has a higher affinity than the Syt1 double mutant, but it is clear that the double mutations helped to close the large gap existing between the membrane affinities of the WT Syt1 and Syt7 C_2A domains. Thus, the ratio between the apparent K_Ds was reduced from more than 200 to 11 (Table 1). These results show that apparently conservative residue substitutions in the membrane-binding regions of C_2 domains can have significant effects on membrane affinity that can accumulate to yield dramatic biochemical and functional differences.

Discussion

Much has been learned about the neurotransmitter release machinery and, among its components, Syts have been studied extensively because of their roles as Ca^{2+} sensors. Although Syt function in release is broadly understood and plausible models for the mechanism of action of Syts in fusion have emerged, the structural determinants that shape the functional differences between fast and slow Syts remain unclear. Particularly intriguing was the observation that disrupting Ca^{2+} binding to the Syt7 C_2A domain impaired its function in asynchronous release much more strongly than disruption of the C_2B domain Ca^{2+} binding sites, in contrast to the opposite effects caused by mutations in the Ca^{2+}-binding sites of the Syt1 C_2 domains on synchronous release (9). The results presented here strongly suggest that the predominant role of the Syt7 C_2A domain in asynchronous release, compared with the C_2B domain, arises because of its stronger contribution to membrane binding, and perhaps to bridging the vesicle and plasma membranes. More generally, our data suggest that the contribution to membrane affinity is a major determinant of the relative functional importance of the C_2 domains of Syts. Furthermore, our results illustrate how small or moderate effects from what appear to be subtle residue substitutions can accumulate to yield dramatic functional differences in Syt C_2 domains.

Ca^{2+}-dependent phospholipid binding was clearly shown to be critical for Syt1 function based on the correlations that were established between the effects of mutations that increase or decrease the apparent Ca^{2+} affinity of Syt1 in the presence of phospholipids and their functional effects on neurotransmitter release (6, 19). This activity is also believed to underlie at least in part the functions of other Ca^{2+}-dependent Syts (5). Hence, our finding that Ca^{2+}-dependent phospholipid binding to Syt7 is dominated by the C_2A domain (Fig. 4) provides a natural explanation for the stronger disruption of asynchronous release caused by mutations in the Ca^{2+}-binding sites of the Syt7 C_2A domain compared with those induced by analogous mutations in the

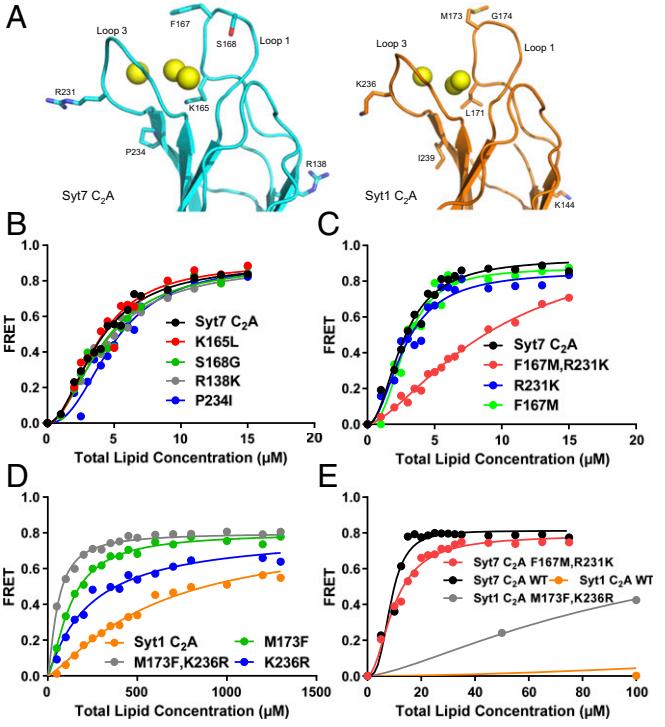

Fig. 7. Subtle residue substitutions underlie in part the stronger membrane binding affinity of the Syt7 C_2A domain compared with the Syt1 C_2A domain. (*A*) Ribbon diagrams of the Syt7 C_2A domain (cyan) and Syt1 C_2A domain (orange) showing the Cα and side chain atoms of residues that are different in their Ca^{2+}-binding regions and were mutated to analyze the basis for their different membrane affinities (oxygens are in red, nitrogens in blue, sulfur atoms in yellow, and carbon atoms in cyan for Syt7 and in orange for Syt1). (*B* and *C*) Titrations of 20 nM WT and mutant Syt7 C_2A domains with liposomes in the presence of 1 mM Ca^{2+}. Binding was monitored from the FRET developed between a donor BODIPY-FL probe attached to the proteins and a rhodamine acceptor present in the liposomes. Each point represents the average of at least three measurements performed with different liposome preparations. (*D*) Analogous liposome titrations of 100 nM WT and mutant Syt1 C_2A domains. (*E*) Analogous liposome titrations of 100 nM WT and mutant Syt1 and Syt7 C_2A domains. Note that the data obtained for WT and M173F,K236R Syt1 C_2A domains (orange and gray circles, respectively) are the same as those shown in *D*, but the scale of the *x* axis is different to allow comparison with the data obtained for the WT and mutant Syt7 C_2A domains. All of the data were fit to a Hill function.

Syt7 C_2B domain (9). Moreover, although the Syt1 C_2A and C_2B domains bind with similar affinities to membranes lacking PIP_2 (Fig. 5), the Syt1 C_2B domain clearly dominates membrane binding in the presence of PIP_2 (Fig. 6), and mutations in the Ca^{2+}-binding sites of the C_2B domain impair membrane binding to Syt1 C_2AB more strongly than mutations in the C_2A domain Ca^{2+} binding sites, in correlation with the functional effects of these mutations (33, 39, 47). A remaining unresolved key issue, however, is the precise role of Ca^{2+}-binding to the Syt1 C_2B-domain. Since the C_2B-domain mutant Syt1 abolishes even asynchronous release in a dominant-negative fashion, although it does not normally mediate such release, such mutant Syt1 likely locks the prefusion complex at the active zone in a Ca^{2+}-unresponsive state, possibly by preventing the Ca^{2+}-dependent unlocking of a complexin-induced prefusion intermediate (48). Although the lack of rescue of Ca^{2+}-dependent release by C_2B-domain mutant Syt1 can thus not be used to argue that Ca^{2+}-dependent phospholipid binding by the Syt1 C_2B-domain is of central importance in release, it seems likely that the "unlocking" of the prefusion complex is actually mediated by Ca^{2+}-dependent phospholipid binding by the Syt1 C_2B-domain. In this sense, Ca^{2+}-dependent phospholipid binding would constitute an intrinsic aspect of Syt1 function even if it did not underlie the differential effects of mutations in the Ca^{2+}-binding sites of the Syt1 C_2 domains, which are opposite to those observed for Syt7.

The intrinsic Ca^{2+} affinities of the C_2A and C_2B domains are similar for both Syt1 and Syt7. What appears to be critical for their relative functional importance is the membrane affinity of the Ca^{2+}-saturated C_2 domain, which is indirectly reflected in the apparent Ca^{2+} affinities observed in Ca^{2+}-dependent phospholipid binding experiments. Thus, the very high affinity of the Ca^{2+}-saturated Syt7 C_2A domain for membranes, dramatically stronger than that of the Syt1 C_2A domain (Figs. 4, 5, and 7), was already reflected in its higher apparent Ca^{2+} affinity (40). Our data show that this dramatic difference in membrane affinity arises in part from cooperative effects resulting from apparently subtle substitutions, including a methionine-to-phenylalanine substitution that is expected to increase hydrophobic interactions with the acyl chains of the membranes and a lysine-to-arginine substitution that is expected to enhance hydrogen bonding to phospholipid headgroups (Fig. 7). It is likely that the overall basic nature of the Syt7 C_2A domain, compared with the acidic nature of the Syt1 C_2A domain (see below), also contributes to the stronger affinity for negatively charged membranes. Regardless of this possibility, the effects of the F167M,R231K mutation in the Syt7 C_2A domain and the reverse M173F,K236R mutation in the Syt1 C_2A domain on membrane binding provide an emphatic illustration of how such subtle mutations can have profound consequences for the biochemical properties of C_2 domains and proteins in general.

Another biochemical property that is intrinsically related to phospholipid binding and could underlie a dominant role for the Syt1 C_2B domain is its ability to bring two membranes into close proximity in a Ca^{2+}-dependent manner (20, 22), which arises because of binding of its Ca^{2+}-binding loops at the top of the β-sandwich to one membrane and interactions of R398 and R399 at the bottom of the sandwich with another membrane, and may also be aided by its basic nature (#basic − #acidic residues = 5). However, there was a priori no clear reason why this property might have switched to the C_2A domain for Syt7. Thus, although the Syt7 C_2A domain (#basic − #acidic residues = 4) is more basic than the Syt1 C_2A domain (#basic − #acidic residues = −2), the Syt7 C_2B domain is even more basic (#basic − #acidic residues = 10) and also contains arginines at the bottom of the β-sandwich. Nevertheless, our DLS measurements (Fig. 4 *D*–*F*) show that the Syt7 C_2A domain does have a much stronger activity in bridging two membranes than the Syt7 C_2B domain. The sequence determinants for this unexpected activity of the Syt7 C_2A domain are currently unclear, but the switch in this property, which is characteristic of the C_2B domain in Syt1 and of the C_2A domain in Syt7, provides a correlation with the critical importance of Ca^{2+} binding to the Syt1 C_2B domain for synchronous release and of Ca^{2+} binding to the Syt7 C_2A domain for asynchronous release. Because Ca^{2+}-dependent bridging of the two membranes could be crucial to trigger Ca^{2+}-dependent fusion, in cooperation with the SNAREs, it is tempting to speculate that this activity is key to determine the relative functional importance of Ca^{2+} binding to the Syt1 and Syt7 C_2 domains. However, it is worth noting that there are other mechanisms by which Ca^{2+}-dependent membrane binding could help to cause membrane fusion, for example by creating tension in the membranes (1), perturbing the packing of the bilayers, or inducing membrane curvature (20, 49).

The notion that membrane affinity or the ability to bridge two membranes might determine the relative contributions of the C_2 domains to Syt function does not imply that other interactions of Syts, such as those with PIP_2 or the SNARE complex, are not important. However, it is worth noting that the primary regions that have been implicated in these interactions [the polybasic region and one face of the β-sandwich of the Syt1 C_2B domain (23–26)] do not include the Ca^{2+}-binding regions, even though Ca^{2+} enhances these interactions. At the high local concentrations of these reagents existing in the primed state of a synaptic vesicle, PIP_2 or SNARE complex binding to the C_2B domain (of either Syt1 or Syt7) could occur in the absence of Ca^{2+} and could help setting up Ca^{2+}-dependent membrane fusion, but the key action of Ca^{2+} binding to Syts that triggers neurotransmitter release is most likely the stimulation of interactions of the Syt Ca^{2+}-binding loops with one or both membranes. Binding of Syt1 to the SNARE complex could facilitate this action, as SNARE complex and membrane binding to Syt1 cooperate with each other (50), but the nature of such cooperation remains unclear given the diversity of Syt1–SNARE complex binding modes observed in recently reported structures (23, 26). Moreover, the interactions observed in these structures involve primarily the Syt1 C_2B domain and the key residues involved in binding are not conserved in the Syt7 C_2A domain. Hence, the mechanisms of coupling of Syt1 and Syt7 with the SNAREs may be more complex than currently envisioned.

Materials and Methods

Recombinant Proteins. N-terminal GST fusion proteins of rat Syt7 fragments 134–262 (C_2A domain), 263–403 (C_2B domain), and 134–403 (C_2AB fragment) were expressed in *Escherichia coli* BL21 (DE3) cells. The bacteria were grown in Lennox L Broth media at 25 °C for 16 h and induced with 0.5 mM isopropyl β-D-1-thiogalactopyranoside. Cells were resuspended in a buffer containing 40 mM Tris·HCl (pH 8.0), 1 M NaCl, 2 mM DTT, 1% Triton and Sigma protease inhibitor mixture (P2714-1BTL), and lysed using an Avestin EmulsiFlex-C5 homogenizer. The soluble fraction of the cell lysate was collected after centrifugation at 48,000 × *g* for 30 min and incubated with 100 mg protamine sulfate (Sigma-Aldrich) per 35 mL supernatant for 1 h at room temperature. The mixture was spun again at 48,000 × *g* for 30 min and the soluble fraction was incubated with Glutathione Sepharose 4B (GE Healthcare) at 4 °C for 16 h. The resin was washed with buffer containing 40 mM Tris·HCl (pH 8.0) and 200 mM NaCl (buffer A), buffer A + 50 mM $CaCl_2$, and buffer A + 50 mM $CaCl_2$ + 1 M NaCl. Remaining nucleic acid contaminants bound to synaptotagmin fragments were then cleared with benzonase treatment (40 units per milliliter of solution, corresponding to ∼1,000 units per liter of cell culture) in 50 mM Tris (pH 8.0), 2 mM $MgCl_2$ for 2 h at room temperature with gentle rotation of the beads. Thrombin cleavage of the GST tag was carried out at room temperature for 3 h in 10 mL thrombin cleavage buffer (50 mM Tris·HCl pH 8.0, 150 mM NaCl, 2.5 mM $CaCl_2$) and 0.08 mg/mL thrombin (Sigma-Aldrich). Eighteen residues from the GST tag (SPGISGGGGGILDSMGRL) remained at the N terminus of Syt7 fragments after thrombin cleavage. Syt7 fragments were further purified with an ion exchange Source S column [buffers: 50 mM NaAc (pH 6.2), 5 mM $CaCl_2$; and 50 mM NaAc (pH 6.2), 5 mM $CaCl_2$, 1 M NaCl]. All proteins were further purified using size-exclusion chromatography on a Superdex 75 16/60 column using buffer containing 20 mM Hepes (pH 7.4), 125 mM KCl, and 1 mM TCEP for Syt7 C_2A and C_2B domains, and buffer containing 20 mM Hepes (pH 7.4), 500 mM NaCl, 1 mM TCEP for the Syt7 C_2AB fragment. Following chromatography, the Syt7 C_2AB fragment was buffer exchanged into 20 mM Hepes (pH 7.4), 125 mM KCl, and 1 mM TCEP by serial concentration and dilution. Syt1 C_2A domain, C_2B domain and C_2AB fragment were purified as

described previously (15, 20, 51, 52). All mutations were performed using the QuikChange site-directed mutagenesis kit (Stratagene). These included the cysteine mutations indicated in the text and the following mutations to disrupt the Ca^{2+}-binding sites: for Syt7 C_2A, D225A,D227A,D233A; for Syt7 C_2B, D357A, D359A; for Syt1 C_2A, D178A,D230A,D232A; for Syt1 C_2B, D309A,D363A,D365A.

Crystallization and X-Ray Data Collection. Purified Syt7 C_2A domain and C_2AB fragment were concentrated to 20 mg/mL in a 20 mM Hepes (pH 7.4), 125 mM KCl, 1 mM $CaCl_2$ buffer, and used for crystal screening. Crystals of Syt7 C_2A domain were grown in 21% t-butanol, 0.1 M Tris (pH 8.5), 0.1 M $CaCl_2$ using the hanging-drop method at 20 °C, and the crystals were cryoprotected by transferring to a final solution of 15% (vol/vol) glycerol, 21% t-butanol, 0.1 M Tris (pH 8.5), 0.1 M $CaCl_2$, then flash-cooled in liquid nitrogen. Crystals of Syt7 C_2AB fragment were grown in 20% PEG 3350, 0.2 M Li_2SO_4, 0.1 M Bis·Tris (pH 6.0), 0.1 M $CaCl_2$ using the hanging-drop method at 20 °C, and the crystals were cryoprotected by transferring to a final solution of 20% (vol/vol) ethylene glycol, 22% PEG 3350, 0.2 M Li_2SO_4, 0.1 M Bis·Tris (pH 6.0), 0.1 M $CaCl_2$.

Data were collected at the APS beamline 19-ID (SBC-CAT) at the Advanced Photon Source (Argonne National Laboratory, Argonne, IL) at 100 K, and were indexed, integrated and scaled using *HKL-3000* (53), with applied corrections for effects resulting from absorption in a crystal and for radiation damage (54, 55), the calculation of an optimal error model, and corrections to compensate the phasing signal for a radiation-induced increase of nonisomorphism within the crystal (56, 57). Syt7 C_2A crystals exhibited the symmetry of space group $P6_5$ with unit cell parameters of a = 55.30 Å, c = 89.81 Å, and contained one molecule of Syt7 C_2A per asymmetric unit, with a solvent content of 50%. Syt7 C_2AB fragment crystals belonged to space group $P2_1$ with unit cell parameters of a = 60.64 Å, b = 75.06 Å, c = 70.98 Å, β = 114.5°, and contained two molecules each of Syt7 C_2AB fragment per asymmetric unit, with a solvent content of 45%. Syt7 C_2A crystals diffracted isotropically to a d_{min} of 1.70 Å when exposed to synchrotron radiation. Syt7 C_2AB fragment crystals diffracted anisotropically to a d_{min} of 2.25 Å when exposed to synchrotron radiation, and displayed strong translational noncrystallographic symmetry characteristic of a pseudo B-centered lattice, as evidenced by a peak in the Patterson function at approximately (1/2, 0, 1/2) with a height ≈49.9% of the origin peak. This resulted in numerous systematically weak reflections in the diffraction pattern, namely for the following reflection conditions: hkl, $h + l = 2n + 1$; hk0, $h = 2n + 1$; 0kl, $l = 2n + 1$; h0l, $h + l = 2n + 1$; 00l, $l = 2n + 1$; and h00, $h = 2n + 1$. Data collection statistics are provided in Table S1.

Phase Determination and Structure Refinement. Phases for the Syt7 C_2A domain were obtained via molecular replacement in the program *Phaser* (58) using a search model derived from the NMR structure of the Ca^{2+}-free Syt7 C_2A domain (PDB ID code 2D8K). Phases for the Syt7 C_2AB fragment were obtained via molecular replacement in the program *Phaser* using search models derived from the structure of the Syt7 C_2A domain described herein and the crystal structure of the Syt7 C_2B domain (PDB ID code 3N5A) (29). Additional protein residues and calcium ions were manually modeled into the electron density maps via the program *COOT* (59). Refinement was performed using the program *Phenix* (60) with a random 5% of all data set aside for an R_{free} calculation. The final model for Syt7 C_2A (R_{work} = 14.4%, R_{free} = 18.1%) contained 138 residues and three Ca^{2+} ions. The final model for Syt7 C_2AB fragment (R_{work} = 21.4%, R_{free} = 25.6%) contained 262 residues in chain A, 263 residues in chain B, and 8 Ca^{2+} ions, or 2 Ca^{2+} ions per C_2 domain. The presence of the pseudocentering operator in the Syt7 C_2AB fragment lattice translates into a systematic modulation of the observed intensities (61, 62) and thus resulted in lower than 100% completeness in the highest resolution shells between 2.70 and 2.25 Å. The *L*-value twinning test (63), which is not influenced by the presence of pseudocentering, shows no significant deviation from the expected values for untwinned data. Ramachandran plots generated with *MolProbity* (64) indicated no outliers in the Ramachandran plot for Syt7 fragments. Data collection and structure refinement statistics are summarized in Table S1. Coordinates and structure factors have been deposited in the Protein Data Bank with ID codes 6ANJ (Syt7 C_2A domain) and 6ANK (Syt7 C_2AB fragment).

Isothermal Titration Calorimetry. The protein solutions were dialyzed twice against the ITC buffer (20 mM Hepes, pH 7.4, 125 mM KCl, 1 mM TCEP). The buffer was pretreated with Chelex-100 (Bio-Rad; calcium binding constant $\approx 4.6 \times 10^3$ M^{-1}) to remove residual calcium ions bound with moderate affinity. The Chelex-100 beads were first washed with water and then added directly to the dialysis buffer for 2 h. The Chelex-100 beads were removed by filtration. The buffer pH was adjusted to 7.4 after filtration. ITC experiments were performed using a VP-ITC system (MicroCal) at 37 °C in ITC buffer. The protein solution (200 μM) was loaded into the sample cell, and $CaCl_2$ solution (20 mM for the Syt7 C_2A domain and 40 mM for the Syt7 C_2B domain) was loaded in the syringe. The $CaCl_2$ solution was prepared by diluting a 1 M stock solution with ITC buffer to the appropriate concentration. $CaCl_2$ was injected at 3-μL volumes 100 times, and the heat evolved per injection was measured. All ITC data were analyzed using the Microcal Origin ITC software packet.

Labeling Proteins with BODIPY-FL Maleimide. Purified proteins at a concentration of 100 μM were incubated with 1 mM BODIPY FL *N*-(2-aminoethyl) maleimide (Molecular Probes) for 2 h at room temperature or for 16 h at 4 °C with rotation. The reaction was quenched by adding 10 mM DTT to the mixture. The unlabeled dye was separated from the labeled protein by ion exchange chromatography on a Source S column (GE Healthcare) [buffers: 50 mM NaAc (pH 6.2), 5 mM $CaCl_2$; and 50 mM NaAc (pH 6.2), 5 mM $CaCl_2$, 1 M NaCl].

Preparation of Phospholipid Vesicles. For preparation of phospholipid vesicles, 1,2-dioleoyl-*sn*-glycero-3-[phospho-L-serine] (DOPS), 1-palmitoyl-2-oleoyl-*sn*-glycero-3-phosphoethanolamine (POPE), 1-palmitoyl-2-oleoyl-*sn*-glycero-3-phosphocholine (POPC), Cholesterol, PIP_2, L-α-phosphatidylinositol (PI), and 1,2-dipalmitoyl-*sn*-glycero-3-phosphoethanolamine-*N*- (lissamine rhodamine B sulfonyl) (ammonium salt; Liss Rho PE; Avanti Polar Lipids) in chloroform were mixed in a glass test tube in a desired ratio, and chloroform was evaporated using a dry nitrogen stream. The lipids were placed in a vacuum chamber overnight for complete removal of organic solvent. Lipid films were hydrated with 20 mM Hepes (pH 7.4) 150 mM KCl buffer in an appropriate volume yielding 10 mM lipids. Lipids were vortexed for >5 min, then frozen and thawed five times. Large unilamellar vesicles were prepared by extruding the hydrated lipid solution through 80 nm polycarbonate membranes 23 times using an Avanti Mini-Extruder. For most FRET assays, we used liposomes containing 41% POPC, 31% POPE, 1% Liss Rho PE, 1% cholesterol, 12% DOPS, and 5% PI. PIP_2-containing liposomes were made by mixing 40% POPC, 31% POPE, 1% Liss Rho PE, 1% cholesterol, 12% DOPS, 1% PIP_2, and 5% PI.

Phospholipid Binding Assays. The FRET experiments were performed at 22 °C on a PTI spectrofluorimeter. All of the experiments were carried out in a buffer containing 20 mM Hepes (pH 7.4) and 150 mM KCl. The labeled protein (20 nM in case of Syt7 fragments and 100 nM in the case of Syt1 fragments, unless otherwise indicated) was mixed with variable amounts of liposomes and 1 mM $CaCl_2$. Note that, although the intrinsic Ca^{2+} affinities of the Syt1 and Syt7 C_2 domains are weak, the apparent Ca^{2+} affinities in the presence of phospholipids are much higher (6, 40), and hence 1 mM Ca^{2+} is sufficient for Ca^{2+} saturation. These samples were excited at 485 nm and the emission spectra from 500 to 600 nm were acquired. A fluorescence spectrum of the same sample after the addition of 2 mM EDTA was also collected. To correct for the bleedthrough from Rhodamine at the emission maxima of BODIPY-FL, a spectrum of liposomes alone was collected and subtracted from the corresponding spectrum acquired in the presence of the protein. The FRET efficiency (E) was calculated with the formula: $E = (I_{EDTA} - I_{Ca})/I_{EDTA}$, where I_{Ca} is the fluorescence intensity of the protein-liposome sample at the emission maxima of BODIPY-FL (512 nm) in the presence of 1 mM Ca^{2+} and I_{EDTA} is the fluorescence intensity of the protein-liposome sample at 512 nm after the addition of 2 mM EDTA. The binding data were fitted to a Hill function using GraphPad PRISM7.

Dynamic Light Scattering. The clustering ability of Syt7 C_2A and C_2B domains was measured by DLS using a DynaPro (Wyatt Technology) instrument equipped with a temperature controlled Microsampler. Liposomes containing 70% POPC and 30% DOPS were used for the DLS experiments. Samples were prepared by mixing 100 μM liposomes and 2 μM protein in 20 mM Hepes, pH 7.4, 125 mM KCl buffer. DLS measurements were made at 22 °C.

NMR Spectroscopy. ^1H-^{15}N HSQC spectra were acquired at 25 °C on Agilent DD2 spectrometers operating at 800 or 600 MHz. Samples contained 30–50 μM uniformly ^{15}N-labeled proteins dissolved in buffer with 20 mM Hepes (pH 7.4), 125 mM KCl containing 5% D_2O. All data were processed with NMRpipe (65) and analyzed with NMRView (66).

ACKNOWLEDGMENTS. We thank Jefferson Knight for fruitful discussions and valuable comments on the mansucript; Thomas Scheuermann for assistance in acquiring the ITC data; and Junjie Xu for help fitting the ITC data. The structures in this report are derived from work performed on beamline 19-ID at the Argonne National Laboratory, Structural Biology Center at the Advanced Photon Source, operated by University of Chicago Argonne, LLC, for the US Department of Energy, Office of Biological and Environmental Research under Contract DE-AC02-06CH11357. The Agilent

DD2 consoles of the 800-MHz spectromenter and one of the 600-MHz spectrometers used for the research presented here were purchased with shared instrumentation grants from the NIH: Grants S10OD018027 (to J.R.) and S10RR026461 (to Michael K. Rosen). R.V. was supported by a fellowship from the Howard Hughes Medical Institute. This work was supported by Grant I-1304 from the Welch Foundation (to J.R.) and by NIH Research Project Award R35 NS097333 (to J.R.), which continues work performed under NIH Grants NS037200 and NS049044 (to J.R.).

1. Südhof TC (2013) Neurotransmitter release: The last millisecond in the life of a synaptic vesicle. *Neuron* 80:675–690.
2. Südhof TC, Rothman JE (2009) Membrane fusion: Grappling with SNARE and SM proteins. *Science* 323:474–477.
3. Rizo J, Xu J (2015) The synaptic vesicle release machinery. *Annu Rev Biophys* 44: 339–367.
4. Brunger AT, Cipriano DJ, Diao J (2015) Towards reconstitution of membrane fusion mediated by SNAREs and other synaptic proteins. *Crit Rev Biochem Mol Biol* 50:231–241.
5. Südhof TC (2002) Synaptotagmins: Why so many? *J Biol Chem* 277:7629–7632.
6. Fernández-Chacón R, et al. (2001) Synaptotagmin I functions as a calcium regulator of release probability. *Nature* 410:41–49.
7. Pang ZP, Sun J, Rizo J, Maximov A, Südhof TC (2006) Genetic analysis of synaptotagmin 2 in spontaneous and Ca2+-triggered neurotransmitter release. *EMBO J* 25:2039–2050.
8. Xu J, Mashimo T, Südhof TC (2007) Synaptotagmin-1, -2, and -9: Ca(2+) sensors for fast release that specify distinct presynaptic properties in subsets of neurons. *Neuron* 54: 567–581.
9. Bacaj T, et al. (2013) Synaptotagmin-1 and synaptotagmin-7 trigger synchronous and asynchronous phases of neurotransmitter release. *Neuron* 80:947–959.
10. Ma C, Su L, Seven AB, Xu Y, Rizo J (2013) Reconstitution of the vital functions of Munc18 and Munc13 in neurotransmitter release. *Science* 339:421–425.
11. Sutton RB, Davletov BA, Berghuis AM, Südhof TC, Sprang SR (1995) Structure of the first C2 domain of synaptotagmin I: A novel Ca2+/phospholipid-binding fold. *Cell* 80:929–938.
12. Shao X, Fernandez I, Südhof TC, Rizo J (1998) Solution structures of the Ca2+-free and Ca2+-bound C2A domain of synaptotagmin I: Does Ca2+ induce a conformational change? *Biochemistry* 37:16106–16115.
13. Fernandez I, et al. (2001) Three-dimensional structure of the synaptotagmin 1 C2B-domain: Synaptotagmin 1 as a phospholipid binding machine. *Neuron* 32:1057–1069.
14. Shao X, Davletov BA, Sutton RB, Südhof TC, Rizo J (1996) Bipartite Ca2+-binding motif in C2 domains of synaptotagmin and protein kinase C. *Science* 273:248–251.
15. Ubach J, Zhang X, Shao X, Südhof TC, Rizo J (1998) Ca2+ binding to synaptotagmin: How many Ca2+ ions bind to the tip of a C2-domain? *EMBO J* 17:3921–3930.
16. Shao X, et al. (1997) Synaptotagmin-syntaxin interaction: The C2 domain as a Ca2+-dependent electrostatic switch. *Neuron* 18:133–142.
17. Zhang X, Rizo J, Südhof TC (1998) Mechanism of phospholipid binding by the C2A-domain of synaptotagmin I. *Biochemistry* 37:12395–12403.
18. Chapman ER, Davis AF (1998) Direct interaction of a Ca2+-binding loop of synaptotagmin with lipid bilayers. *J Biol Chem* 273:13995–14001.
19. Rhee JS, et al. (2005) Augmenting neurotransmitter release by enhancing the apparent Ca2+ affinity of synaptotagmin 1. *Proc Natl Acad Sci USA* 102:18664–18669.
20. Araç D, et al. (2006) Close membrane-membrane proximity induced by Ca(2+)-dependent multivalent binding of synaptotagmin-1 to phospholipids. *Nat Struct Mol Biol* 13:209–217.
21. Xue M, Ma C, Craig TK, Rosenmund C, Rizo J (2008) The Janus-faced nature of the C(2)B domain is fundamental for synaptotagmin-1 function. *Nat Struct Mol Biol* 15:1160–1168.
22. Seven AB, Brewer KD, Shi L, Jiang QX, Rizo J (2013) Prevalent mechanism of membrane bridging by synaptotagmin-1. *Proc Natl Acad Sci USA* 110:E3243–E3252.
23. Brewer KD, et al. (2015) Dynamic binding mode of a synaptotagmin-1-SNARE complex in solution. *Nat Struct Mol Biol* 22:555–564.
24. Bai J, Tucker WC, Chapman ER (2004) PIP2 increases the speed of response of synaptotagmin and steers its membrane-penetration activity toward the plasma membrane. *Nat Struct Mol Biol* 11:36–44.
25. Li L, et al. (2006) Phosphatidylinositol phosphates as co-activators of Ca2+ binding to C2 domains of synaptotagmin 1. *J Biol Chem* 281:15845–15852.
26. Zhou Q, et al. (2015) Architecture of the synaptotagmin-SNARE machinery for neuronal exocytosis. *Nature* 525:62–67.
27. Dai H, et al. (2004) Structural basis for the evolutionary inactivation of Ca2+ binding to synaptotagmin 4. *Nat Struct Mol Biol* 11:844–849.
28. Schonn JS, Maximov A, Lao Y, Südhof TC, Sørensen JB (2008) Synaptotagmin-1 and -7 are functionally overlapping Ca2+ sensors for exocytosis in adrenal chromaffin cells. *Proc Natl Acad Sci USA* 105:3998–4003.
29. Xue M, et al. (2010) Structural and mutational analysis of functional differentiation between synaptotagmins-1 and -7. *PLoS One* 5:e12544.
30. Mackler JM, Drummond JA, Loewen CA, Robinson IM, Reist NE (2002) The C(2)B Ca(2+)-binding motif of synaptotagmin is required for synaptic transmission in vivo. *Nature* 418: 340–344.
31. Robinson IM, Ranjan R, Schwarz TL (2002) Synaptotagmins I and IV promote transmitter release independently of Ca(2+) binding in the C(2)A domain. *Nature* 418:336–340.
32. Nishiki T, Augustine GJ (2004) Dual roles of the C2B domain of synaptotagmin I in synchronizing Ca2+-dependent neurotransmitter release. *J Neurosci* 24:8542–8550.
33. Shin OH, Xu J, Rizo J, Südhof TC (2009) Differential but convergent functions of Ca2+ binding to synaptotagmin-1 C2 domains mediate neurotransmitter release. *Proc Natl Acad Sci USA* 106:16469–16474.
34. Wu D, et al. (2017) Postsynaptic synaptotagmins mediate AMPA receptor exocytosis during LTP. *Nature* 544:316–321.
35. Rizo J, Südhof TC (1998) C2-domains, structure and function of a universal Ca2+-binding domain. *J Biol Chem* 273:15879–15882.
36. Maximov A, et al. (2008) Genetic analysis of synaptotagmin-7 function in synaptic vesicle exocytosis. *Proc Natl Acad Sci USA* 105:3986–3991.
37. Fuson KL, Montes M, Robert JJ, Sutton RB (2007) Structure of human synaptotagmin 1 C2AB in the absence of Ca2+ reveals a novel domain association. *Biochemistry* 46: 13041–13048.
38. Sutton RB, Ernst JA, Brunger AT (1999) Crystal structure of the cytosolic C2A-C2B domains of synaptotagmin III. Implications for Ca(+2)-independent snare complex interaction. *J Cell Biol* 147:589–598.
39. Radhakrishnan A, Stein A, Jahn R, Fasshauer D (2009) The Ca2+ affinity of synaptotagmin 1 is markedly increased by a specific interaction of its C2B domain with phosphatidylinositol 4,5-bisphosphate. *J Biol Chem* 284:25749–25760.
40. Shin OH, Rizo J, Südhof TC (2002) Synaptotagmin function in dense core vesicle exocytosis studied in cracked PC12 cells. *Nat Neurosci* 5:649–656.
41. Brandt DS, Coffman MD, Falke JJ, Knight JD (2012) Hydrophobic contributions to the membrane docking of synaptotagmin 7 C2A domain: Mechanistic contrast between isoforms 1 and 7. *Biochemistry* 51:7654–7664.
42. Hui E, et al. (2005) Three distinct kinetic groupings of the synaptotagmin family: Candidate sensors for rapid and delayed exocytosis. *Proc Natl Acad Sci USA* 102: 5210–5214.
43. Frazier AA, Roller CR, Havelka JJ, Hinderliter A, Cafiso DS (2003) Membrane-bound orientation and position of the synaptotagmin I C2A domain by site-directed spin labeling. *Biochemistry* 42:96–105.
44. Rufener E, Frazier AA, Wieser CM, Hinderliter A, Cafiso DS (2005) Membrane-bound orientation and position of the synaptotagmin C2B domain determined by site-directed spin labeling. *Biochemistry* 44:18–28.
45. Rizo J, Rosenmund C (2008) Synaptic vesicle fusion. *Nat Struct Mol Biol* 15:665–674.
46. Chapman ER (2008) How does synaptotagmin trigger neurotransmitter release? *Annu Rev Biochem* 77:615–641.
47. van den BG, Meyenberg K, Diederichsen U, Jahn R (2012) Phosphatidylinositol 4,5-bisphosphate increases Ca2+ affinity of synaptotagmin-1 by 40-fold. *J Biol Chem* 287: 16447–16453.
48. Tang J, et al. (2006) A complexin/synaptotagmin 1 switch controls fast synaptic vesicle exocytosis. *Cell* 126:1175–1187.
49. Martens S, Kozlov MM, McMahon HT (2007) How synaptotagmin promotes membrane fusion. *Science* 316:1205–1208.
50. Dai H, Shen N, Araç D, Rizo J (2007) A quaternary SNARE-synaptotagmin-Ca2+-phospholipid complex in neurotransmitter release. *J Mol Biol* 367:848–863.
51. Ubach J, et al. (2001) The C2B domain of synaptotagmin I is a Ca2+-binding module. *Biochemistry* 40:5854–5860.
52. Zhou A, Brewer KD, Rizo J (2013) Analysis of SNARE complex/synaptotagmin-1 interactions by one-dimensional NMR spectroscopy. *Biochemistry* 52:3446–3456.
53. Minor W, Cymborowski M, Otwinowski Z, Chruszcz M (2006) HKL-3000: The integration of data reduction and structure solution—From diffraction images to an initial model in minutes. *Acta Crystallogr D Biol Crystallogr* 62:859–866.
54. Borek D, Minor W, Otwinowski Z (2003) Measurement errors and their consequences in protein crystallography. *Acta Crystallogr D Biol Crystallogr* 59:2031–2038.
55. Otwinowski Z, Borek D, Majewski W, Minor W (2003) Multiparametric scaling of diffraction intensities. *Acta Crystallogr A* 59:228–234.
56. Borek D, Cymborowski M, Machius M, Minor W, Otwinowski Z (2010) Diffraction data analysis in the presence of radiation damage. *Acta Crystallogr D Biol Crystallogr* 66: 426–436.
57. Borek D, Dauter Z, Otwinowski Z (2013) Identification of patterns in diffraction intensities affected by radiation exposure. *J Synchrotron Radiat* 20:37–48.
58. McCoy AJ, et al. (2007) Phaser crystallographic software. *J Appl Cryst* 40:658–674.
59. Emsley P, Cowtan K (2004) Coot: Model-building tools for molecular graphics. *Acta Crystallogr D Biol Crystallogr* 60:2126–2132.
60. Adams PD, et al. (2010) PHENIX: A comprehensive Python-based system for macromolecular structure solution. *Acta Crystallogr D Biol Crystallogr* 66:213–221.
61. Zwart PH, Grosse-Kunstleve RW, Lebedev AA, Murshudov GN, Adams PD (2008) Surprises and pitfalls arising from (pseudo)symmetry. *Acta Crystallogr D Biol Crystallogr* 64:99–107.
62. Chook YM, Lipscomb WN, Ke H (1998) Detection and use of pseudo-translation in determination of protein structures. *Acta Crystallogr D Biol Crystallogr* 54:822–827.
63. Padilla JE, Yeates TO (2003) A statistic for local intensity differences: Robustness to anisotropy and pseudo-centering and utility for detecting twinning. *Acta Crystallogr D Biol Crystallogr* 59:1124–1130.
64. Chen VB, et al. (2010) MolProbity: All-atom structure validation for macromolecular crystallography. *Acta Crystallogr D Biol Crystallogr* 66:12–21.
65. Delaglio F, et al. (1995) NMRPipe: A multidimensional spectral processing system based on UNIX pipes. *J Biomol NMR* 6:277–293.
66. Johnson BA, Blevins RA (1994) NMR View: A computer program for the visualization and analysis of NMR data. *J Biomol NMR* 4:603–614.